Laser-free trapped-ion entangling gates with simultaneous insensitivity to qubit and motional decoherence

R. T. Sutherland [1,*] R. Srinivas,[2,3] S. C. Burd [2,3] H. M. Knaack [2,3] A. C. Wilson,[2] D. J. Wineland,[2,3,4] D. Leibfried,[2] D. T. C. Allcock [2,3,4] D. H. Slichter,[2] and S. B. Libby [1]

[1]*Physics Division, Physical and Life Sciences, Lawrence Livermore National Laboratory, Livermore, California 94550, USA*
[2]*Time and Frequency Division, National Institute of Standards and Technology, 325 Broadway, Boulder, Colorado 80305, USA*
[3]*Department of Physics, University of Colorado, Boulder, Colorado 80309, USA*
[4]*Department of Physics, University of Oregon, Eugene, Oregon 97403, USA*

The dominant error sources for state-of-the-art laser-free trapped-ion entangling gates are decoherence of the qubit state and the ion motion. The effect of these decoherence mechanisms can be suppressed with additional control fields or with techniques that have the disadvantage of reducing gate speed. Here, we propose using a near-motional-frequency magnetic field gradient to implement a laser-free gate that is simultaneously resilient to both types of decoherence, does not require additional control fields, and has a relatively small cost in gate speed.

I. INTRODUCTION

Trapped ions are a promising platform for quantum simulations and universal quantum computation due to their long coherence times, inherent uniformity, and high gate fidelities [1–8]. The most common method for performing high-fidelity multiqubit entangling gates, a requirement for universal quantum processors, relies on coupling the internal qubit "spin" states to collective motional degrees of freedom [1,2,9]. Geometric phase gates—which create entanglement through closed, spin-dependent trajectories in motional phase space—are widely used because they are first order insensitive to ion temperature (in the Lamb-Dicke limit) [10–12]. Geometric phase gates employing laser beams to create the required spin-motion coupling have been used to generate Bell states with fidelities of ∼0.999 [7,8], with the main error arising from off-resonant photon scattering [13]. Alternative laser-free schemes induce spin-motion coupling with static [14–19], near-qubit-frequency [20–25], or near-motional-frequency [20,26–28] magnetic field gradients. While laser-free schemes eliminate photon scattering errors and do not require stable, high-power lasers, they can be more susceptible to other noise sources due to their typically longer gate durations.

Qubit frequency shifts or miscalibrations due to fluctuating field amplitudes are the primary sources of error in laser-free gates implemented with microwave field gradients [19,21]. Recent work has shown that some of these shifts may be reduced passively through careful trap design [24]. They can also be reduced actively by adding control fields to perform dynamical decoupling [18,29–32]; to date, the best

experimentally demonstrated Bell state fidelity using such a scheme is 0.997(1) [22]. Schemes which employ static magnetic field gradients to perform laser-free gates allow high-fidelity individual addressing of the ions in frequency space [33]; however, this means that the microwave frequencies needed to realize an entangling gate are different for each ion, increasing the total number of drive tones necessary to implement such a gate [18,19].

Since laser-free geometric phase gates are typically slower than laser-based gates by an order of magnitude, the qubits spend more time entangled with the motional mode, and thus, the gates are more sensitive to motional decoherence. Typically, after qubit frequency shifts, this is the next most important source of gate error [18,22,24]. In the work reported here, we consider motional decoherence in three distinct regimes, depending on the timescale and nature of the decoherence: secular frequency shifts, motional heating, and motional dephasing.

In their original proposal, Sørensen and Mølmer pointed out that dividing a geometric phase gate into K loops decreases gate errors from heating and motional dephasing [11]. Separately, decoherence from secular frequency shifts can be suppressed with Walsh sequences [34] or with phase modulation of gate fields [35,36]. These techniques increase the gate duration t_G in exchange for robustness. Polychromatic gates [37], geometric phase gates composed of multiple simultaneously applied gate fields with optimized amplitudes, reduce the impact of all three types of motional decoherence and have a comparatively smaller increase in t_G. This technique was recently demonstrated for both laser-based [38] and laser-free gates [19]. These gate implementations, however, remain sensitive to qubit frequency offsets, although they provide some dynamical decoupling for zero-mean fluctuations; their physical implementation also requires additional control

*sutherland11@llnl.gov

fields, increasing experimental complexity. Similar robustness to motional errors can alternatively be achieved by smooth ramping of the gate field amplitude over the entire duration of the gate pulse [25].

In this work, we build upon Ref. [27] to propose a gate that provides simultaneous robustness to qubit frequency shifts and to motional decoherence without requiring additional control fields, offering a combination of increased fidelity and decreased experimental overhead. The protection from qubit frequency errors extends to much larger frequency offsets than can typically be protected against using dynamical decoupling techniques because the entangling gate commutes with these fluctuations, unlike all other laser-free entangling gates demonstrated previously.

The outline of the paper is as follows. In Sec. II we present a theoretical framework we use to analyze the qubit dynamics generated by a pair of microwave fields symmetrically detuned around the qubit frequency and a near-motional-frequency magnetic field gradient. In Sec. III, we show how to tune these control fields to realize a geometric phase gate which is insensitive to qubit frequency shifts and robust to motional decoherence. We also characterize its performance with numerical simulations. In Sec. VII, we analyze poly-chromatic gates that use multiple pairs of microwave fields and contrast them with the scheme presented here. Finally, we present conclusions and prospects for future work.

II. BICHROMATIC INTERACTION PICTURE FOR LASER-FREE GATES

We consider a Hamiltonian for laser-free gates between two trapped ions with identical qubit frequencies ω_0, coupled to a shared motional mode with frequency ω_r. We apply a pair of microwave-frequency magnetic fields (symmetrically detuned around ω_0 by $\pm\delta$) and a separate magnetic field gradient oscillating at ω_g, where $\omega_g \approx \frac{1}{3}\omega_r$, as shown in Fig. 1(a). Neglecting noise, the dynamics of this system are governed by the Hamiltonian

$$\hat{H}_{\text{lab}}(t) = \frac{\hbar\omega_0}{2}\hat{S}_z + \hbar\omega_r\hat{a}^\dagger\hat{a} + 2\hbar\Omega_g\cos(\omega_g t)\hat{S}_z\{\hat{a} + \hat{a}^\dagger\} + 2\hbar\Omega_\mu\hat{S}_x\{\cos([\omega_0 + \delta]t) + \cos([\omega_0 - \delta]t)\}, \quad (1)$$

where Ω_g is the magnetic-field-gradient Rabi frequency and Ω_μ is the microwave Rabi frequency. We define two-ion Pauli spin operators as $\hat{S}_\gamma \equiv \hat{\sigma}_{\gamma,1} + \hat{\sigma}_{\gamma,2}$, with $\gamma \in \{x, y, z, +, -\}$ and z being the qubit quantization axis. The shared ion motion has creation and annihilation operators $\hat{a}^\dagger$ and $\hat{a}$. This Hamiltonian can be generalized to multiple pairs of microwave tones or arbitrary gradient time dependence without significant complication (see Appendix A). Transforming into the interaction frame with respect to $\hat{H}_0 = \hbar\omega_0\hat{S}_z/2 + \hbar\omega_r\hat{a}^\dagger\hat{a}$ and ignoring terms that oscillate with frequencies near $2\omega_0$ give

$$\hat{H}(t) = 2\hbar\Omega_\mu\hat{S}_+\cos(\delta t) + 2\hbar\Omega_g\cos(\omega_g t)\hat{S}_z\hat{a}e^{-i\omega_r t} + \text{H.c.} \quad (2)$$

The oscillating gradient at ω_g, in combination with the detuned microwaves, can give rise to two spin-motion-coupling sideband interactions, occurring when $\delta = \omega_r \pm \omega_g$ [28]. The
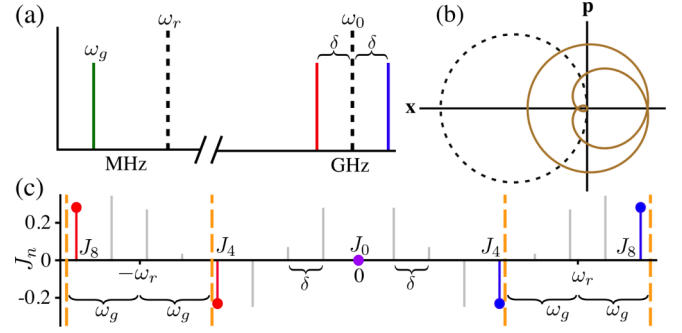

FIG. 1. (a) Frequency spectrum of the three fields used to perform the described gates. (b) Motional phase-space trajectories of two gates that are insensitive to qubit frequency shifts. The black dashed line represents a conventional single-tone gate [12], and the brown solid line corresponds to a motionally robust gate proposed in this work. (c) For the arguments described in the text, amplitudes of Bessel functions J_n versus frequency in the rotating frame of the qubit. The dynamics of the bichromatic microwave pair gives an effective modulation of the microwave Rabi frequency and causes a series of resonances at integer multiples of δ with strength proportional to the corresponding Bessel function. A polychromatic gate occurs when two resonances (here J_4 and J_8) are tuned near $|\omega_r \pm \omega_g|$.

proposed gate relies on this feature of the interaction, along with the fact that the bichromatic microwave pair combines to give an effective modulation of Ω_μ. This scheme requires a magnetic-field-sensitive qubit transition instead of the magnetic-field-insensitive "clock" transitions typically preferred for their long coherence times. We envision storing quantum information in a clock qubit and transferring the state populations to a field-sensitive qubit only during times when an entangling gate is being carried out. Alternatively, microwave fields can be applied to field-sensitive transitions to create dressed-state clock qubits [31].

Typical experimental values of the amplitude $\Omega_g/2\pi$ are in the few-kilohertz regime, whereas $\Omega_\mu/2\pi$ can be in the megahertz regime [28]. It is therefore convenient to analyze the system dynamics in a frame that eliminates the large size disparity between the terms. This can be done by transforming into the interaction picture with respect to the bichromatic microwaves [27,39,40]:

$$\hat{H}_I(t) = \hat{U}^\dagger(t)\hat{H}(t)\hat{U}(t) + i\hbar\hat{U}^\dagger(t)\dot{\hat{U}}(t), \quad (3)$$

where the frame transformation $\hat{U}(t)$, given by

$$\hat{U}(t) = \exp\left\{-i\hat{S}_x\frac{\Omega_\mu\sin(\delta t)}{\delta}\right\}, \quad (4)$$

encapsulates the dynamics of the microwave pair (see Appendix B). In the time-dependent transformed basis of this "bichromatic" interaction picture, the system dynamics between times t_i and t_f, given by the propagator $\hat{T}_I(t_i, t_f)$ of $\hat{H}_I(t)$, appear to be simplified. Crucially, however, if the microwave pair (as parameterized by Ω_μ) can be turned on and off in such a manner that $\hat{U}(t_i) = \hat{I}$ and $\hat{U}(t_f) = \hat{I}$, where $\hat{I}$ is the identity operator, then the state evolution given by $\hat{T}_I(t_i, t_f)$ applies to the laboratory frame basis as well as the transformed basis in the bichromatic interaction picture. This

condition on $\hat{U}(t_i)$ and $\hat{U}(t_f)$ can be achieved by ramping the microwave pair on and off slowly with respect to $1/\delta$ or by choosing the gate duration t_G (during which the microwave pair is on) such that $t_G\delta$ is an integer multiple of 2π. Either method can be used, with realistic parameters, such that the fidelities of the final state in the laboratory frame basis and the interaction frame basis differ by less than 10^{-4}. While the first method would be used in experiments, we use the second method in this paper (unless otherwise specified) because it is simpler for the numerical simulations. Making the above transformation on Eq. (2) gives [27]

$$\hat{H}_I(t) = 2\hbar\Omega_g \cos(\omega_g t)\{\hat{a}e^{-i\omega_r t} + \hat{a}^\dagger e^{i\omega_r t}\}$$

$$\times \left\{ \hat{S}_z\left[J_0\left(\frac{4\Omega_\mu}{\delta}\right) + 2\sum_{n=1}^{\infty} J_{2n}\left(\frac{4\Omega_\mu}{\delta}\right)\cos(2n\delta t) \right] \right.$$

$$\left. + 2\hat{S}_y \sum_{n=1}^{\infty} J_{2n-1}\left(\frac{4\Omega_\mu}{\delta}\right)\sin([2n-1]\delta t) \right\}. \quad (5)$$

We also note that, for simplicity, we have assumed all single-qubit operations implemented in this work are instantaneous and error free.

III. POLYCHROMATIC GATES

In this section, we discuss a protocol for tuning Eq. (5) to represent an entangling gate that is insensitive to motional and qubit decoherence. By setting the conditions

$$4\delta = (\omega_r - \omega_g) - j\Delta,$$
$$8\delta = (\omega_r + \omega_g) - (j+1)\Delta, \quad (6)$$

where j is an integer and $\Delta = 2\pi/t_G$ is on the order of Ω_g, the terms $\propto J_4$ and $\propto J_8$ become slowly varying in time with respect to all other terms in the sum. They will thus make the dominant contribution to the system dynamics, while the other terms that appear in Eq. (5) are significantly off resonant, with contributions scaling as $(\Omega_g/\delta)^2$, where we note that $\Omega_g \ll \delta$. In the laboratory frame, the conditions in Eq. (6) are equivalent to setting δ and ω_g to predominantly drive both the $\omega_r - \omega_g$ and $\omega_r + \omega_g$ sidebands simultaneously, as shown in Fig. 1(c).

Keeping only these near-resonant terms gives

$$\hat{H}_I(t) \simeq \hbar\Omega_g \hat{S}_z \left\{ J_4\left(\frac{4\Omega_\mu}{\delta}\right)(\hat{a}e^{-ij\Delta t} + \hat{a}^\dagger e^{ij\Delta t}) \right.$$

$$\left. + J_8\left(\frac{4\Omega_\mu}{\delta}\right)(\hat{a}e^{-i(j+1)\Delta t} + \hat{a}^\dagger e^{i(j+1)\Delta t}) \right\}, \quad (7)$$

which resembles the form of the motionally robust polychromatic gates discussed in Refs. [19,37,38]. This will generate a gate with K loops if we choose

$$\Delta = 4\Omega_g K^{1/2} \left\{ \frac{\left[J_4\left(\frac{4\Omega_\mu}{\delta}\right)\right]^2}{j} + \frac{\left[J_8\left(\frac{4\Omega_\mu}{\delta}\right)\right]^2}{j+1} \right\}^{1/2}. \quad (8)$$

Since $J_4(4\Omega_\mu/\delta)$ and $J_8(4\Omega_\mu/\delta)$ are independent functions, we may optimize the amplitudes of their effective tones by setting the value of Ω_μ/δ. For example, when $j = 1$, we can engineer a gate that is robust to gate duration errors

when $J_8(4\Omega_\mu/\delta)/J_4(4\Omega_\mu/\delta) = -1$ [38] or the motionally robust gates of Refs. [19,37] when $J_8(4\Omega_\mu/\delta)/J_4(4\Omega_\mu/\delta) = -2$ [37]. These gates are, unfortunately, still sensitive to time-varying qubit frequency shifts.

IV. QUBIT DECOHERENCE

We model the effects of time-dependent qubit frequency shifts by adding a term $\hat{H}_z(t) \equiv (\hbar\varepsilon/2)\cos(\omega_\varepsilon t)\hat{S}_z^{(\prime)}$ to the ideal Hamiltonian in Eq. (2). Here, we introduce an antisymmetric two-qubit Pauli operator $\hat{S}_z' \equiv \hat{\sigma}_{z,1} - \hat{\sigma}_{z,2}$ in order to represent a differential qubit shift. In the bichromatic interaction picture, keeping only near-resonant terms (assuming $\varepsilon, \omega_\varepsilon \ll \delta$), $\hat{H}_{z,I}(t)$ can be written as

$$\hat{H}_{z,I}(t) \simeq \frac{\hbar\varepsilon}{2} J_0\left(\frac{4\Omega_\mu}{\delta}\right)\cos(\omega_\varepsilon t)\hat{S}_z^{(\prime)}. \quad (9)$$

Note that the above equation is valid for symmetric and antisymmetric Pauli operators. When the value of $4\Omega_\mu/\delta$ is set to one of the zeros of the J_0 Bessel function, the expression in Eq. (9) goes to zero, and the qubit frequency shifts do not contribute to the dynamics. The off-resonant terms dropped from Eq. (9) all oscillate at integer multiples of δ, such that in the typical case where $\varepsilon, \omega_\varepsilon \ll \delta$, their effect averages to zero; we refer to this phenomenon as intrinsic dynamical decoupling (IDD) [27]. By tuning δ, ω_g, and ω_r so that Eqs. (6) are met for a particular value of j and setting $4\Omega_\mu/\delta \simeq 8.65$, the third IDD point [i.e., the third zero of $J_0(4\Omega_\mu/\delta)$], we perform a gate such that $J_8(4\Omega_\mu\delta)/J_4(4\Omega_\mu/\delta) \simeq -1.22$ [see Fig. 1(c)]; we will refer to this as the IDD-j gate. The phase-space trajectory of an IDD-2 gate is shown in Fig. 1(b). Figure 1(b) also compares the IDD-2 gate's trajectory to that of a single-tone $\hat{\sigma}_z\hat{\sigma}_z$ gate corresponding to the J_2 resonance performed at the first IDD point (here referred to as IDD-single) [27]. While the phase-space trajectories of IDD-single and IDD-1 gates are not completely centered on the origin, those of IDD-j gates for $j \geq 2$ are, resulting in less time-averaged spin-motion entanglement and, consequently, less impact of motional decoherence on gate fidelity. For all the calculations shown, we use experimentally achievable values of $\Omega_g/2\pi = 1$ kHz and $\omega_r/2\pi = 6.5$ MHz. Here, $\omega_g/2\pi = 5$ MHz for the IDD-single gate; for the IDD-j gates, ω_g is determined by solving Eqs. (6) and (8), giving $\omega_g \sim \omega_r/3$.

In addition to the intrinsic dynamical decoupling effect described above, the IDD-j gates can also be made highly insensitive to static qubit frequency shifts. These gates produce an effective interaction of the form $\sigma_{z,1}\sigma_{z,2}$, such that qubit frequency shifts as shown in Eq. (9) commute with the gate operation. As a result, the effect of static shifts can be removed (when $\varepsilon \ll \delta$) by performing a $K = 2$ loop gate with a qubit π rotation in between loops (a Walsh modulation of index 1) [34]. Figures 2(a) and 2(b) show numerical simulations [including all terms in Eq. (2)] of the impact of symmetric ($\propto \hat{S}_z$) and antisymmetric ($\propto \hat{S}_z'$) static shifts, respectively, on the fidelity $\mathcal{F}$. Both of these show that the fidelity of our gates is unaffected by static frequency shifts at the 10^{-4} level for $\varepsilon \lesssim 300\,\Omega_g$. Note that the insensitivity to antisymmetric qubit frequency shifts implies that individual qubit addressing in frequency space should be possible with this scheme. We define the fidelity as $\mathcal{F} \equiv \langle\Phi^+|\hat{\rho}(t_G)|\Phi^+\rangle$, where $|\Phi^+\rangle \equiv$

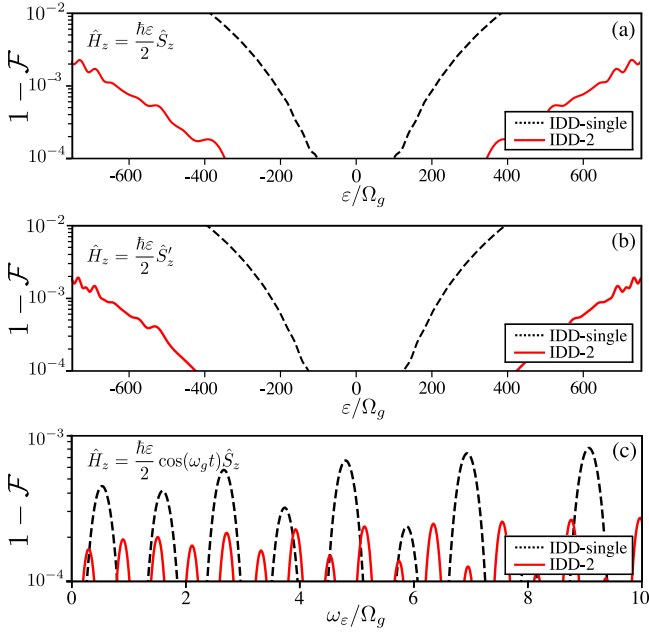FIG. 2. (a) Gate infidelity $1 - \mathcal{F}$ (plotted logarithmically) versus symmetric qubit frequency offset ε for IDD-single (black dashed line) and IDD-2 (solid red line) gates with a given gradient strength Ω_g. (b) Gate infidelity $1 - \mathcal{F}$ versus antisymmetric qubit frequency offset ε for IDD-single (black dashed line) and IDD-2 (solid red line) gates with a given gradient strength Ω_g. (c) Gate infidelity $1 - \mathcal{F}$ for the same gates versus the frequency ω_ε of a symmetric qubit frequency shift, with $\varepsilon = \Omega_g/5$. Every simulated gate has two phase-space loops with a global qubit π rotation in between.

$1/\sqrt{2}(|\downarrow\downarrow\rangle + i |\uparrow\uparrow\rangle)$ is the target qubit state when starting in $|\downarrow\downarrow\rangle$ and performing global $\pi/2$ rotations (perpendicular to $\hat{z}$) immediately before and after the $\sigma_{z,1}\sigma_{z,2}$ gate. This technique breaks down as ε approaches δ, such that the off-resonant terms that were dropped in Eq. (9) become non-negligible. Figure 2 also makes a comparison to the IDD-single gate proposed in Ref. [27]. Sensitivity to oscillating qubit frequency shifts is shown in Fig. 2(c), where we plot the infidelity $1 - \mathcal{F}$ versus ω_ε assuming a shift amplitude $\varepsilon = \Omega_g/5$. For $1 - \mathcal{F} \ll 1$, the infidelity scales as ε^2. The numerical simulations shown in Fig. 2 use a 20-μs Blackman envelope to shape the rising and falling edges of the gradient pulses and the microwave pulses [41]. We turn on the microwave pair first, ramping up the gradient after the microwaves reach steady state, and ramp down in the reverse order at the end of the pulses. This is done because the gate speed is linear in the gradient strength, while it depends on the microwave amplitude as the argument of the two Bessel functions J_4 and J_8 [see Eq. (7)], causing complicated undesired dynamics during the microwave ramp if the gradient is already present. The errors seen in Fig. 2(c) occur during the microwave rise and fall times, when Ω_μ is not at the IDD point, such that the qubits are vulnerable to frequency fluctuations of the form in $\hat{H}_z(t)$. We note that qubit shifts that oscillate at or near $n\delta$ (for integer n) appear in the bichromatic interaction picture as static error terms $\propto \hat{S}_z$ (for even n) or $\propto \hat{S}_y$ (for odd n) [27]. Experimentally, qubit frequency fluctuations near $n\delta$ can arise from residual magnetic fields at ω_g from the currents generating the gra-
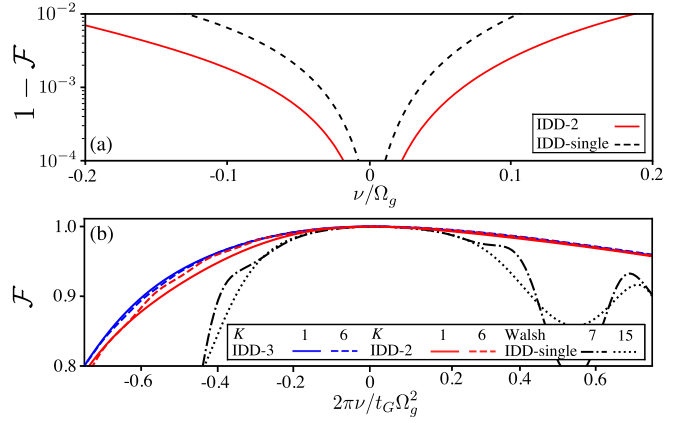

FIG. 3. (a) Gate infidelity $1 - \mathcal{F}$ (plotted logarithmically) versus motional frequency offset ν for both of the qubit-frequency-shift-resistant gates shown in Fig. 2, given a fixed gradient Ω_g. Both gates shown here undergo two phase-space loops with a global qubit π rotation in between. (b) Comparison of IDD-single gates performed with Walsh modulation of index 7 or 15 ($K = 8$ and $K = 16$, respectively) to IDD-2 and IDD-3 gates with $K = 1$ or $K = 6$, plotted against a dimensionless motional offset ν/Ω_g normalized by a dimensionless gate duration $t_G\Omega_g/2\pi$. All IDD gates fall on a similar curve, as do IDD-single gates for small values of $2\pi\nu/t_G\Omega_g^2$.

dient. Choosing the J_4 and J_8 resonances to implement the gate makes n even, so the resulting errors are $\propto \hat{S}_z$ and can be removed as described below (see Sec. VI).

V. MOTIONAL DECOHERENCE

Gates with multiple blue and red sideband pairs, such as those presented in this work, have reduced sensitivity to motional frequency offsets. For example, an IDD-j gate is a linear superposition of a j and a $j + 1$ loop IDD-single gate, each with amplitudes of opposite signs. A motional frequency offset ν shifts the secular frequency such that $\omega_r \to \omega_r + \nu$, resulting in a residual displacement in phase space at the end of the gate. With nonzero ν, the superposed gates experience opposite displacements in phase space which coherently cancel each other. As shown in Fig. 3(a), this results in reduced sensitivity to ν [19,38]. Figure 3(b) shows that this coherent error cancellation can provide reduced sensitivity to ν by increasing either the number of loops K or the order j of the gate. The infidelity due to an offset ν will remain constant for an increased ν if t_G is also increased proportionally; this remains true whether the increased t_G is associated with more loops K or larger values of j. In Fig. 3(b), we plot Bell state infidelity for a variety of different gates versus the dimensionless motional frequency offset ν/Ω_g, normalized by the dimensionless gate duration $t_G\Omega_g/2\pi$. With this normalization, the different gates fall on approximately the same curve of sensitivity to motional frequency offsets. As the gate-time-normalized motional frequency offset becomes larger, the IDD-j gates have higher fidelity than single-tone gates following Walsh sequences, shown in Fig. 3(b) [34].

In Fig. 4, we show the increased robustness to heating and motional dephasing of the IDD-j gates. We treat these decoherence mechanisms as Markovian, using a Lindblad
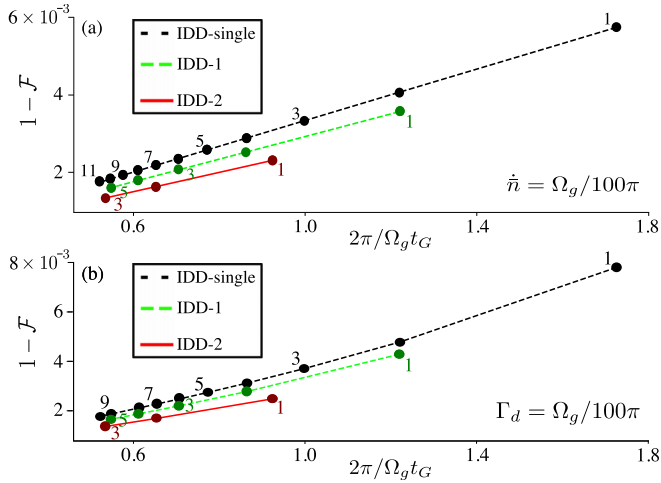
FIG. 4. (a) Infidelity $1 - \mathcal{F}$ due to motional heating versus normalized gate speed $2\pi/\Omega_g t_G$. Point labels indicate the number of phase-space loops K. For a given gradient strength Ω_g and heating rate $\dot{n} = \Omega_g/100\pi$, the error of a gate scales with $1/t_G$. For a given t_G, the IDD-2 (solid red line) and IDD-1 (dashed green line) gates outperform the IDD-single (dashed black line) gate. Higher-order IDD-j gates for $j \geqslant 3$ are similar to the IDD-2 gate. (b) shows the same calculations for motional dephasing instead of motional heating, assuming a motional dephasing rate of $\Gamma_d = \Omega_g/100\pi$.

formalism [42]. Note that for these calculations, we use Eq. (7) to calculate the infidelity; this gives the same motional decoherence effect as the full integration of Eq. (2) (see Appendix D). Geometric phase gates can be made less sensitive to motional heating by performing more phase-space loops, with $1 - \mathcal{F}$ scaling $\propto 1/t_G$. Therefore, in order to make a relevant comparison to our polychromatic gates, Fig. 4(a) shows the infidelity due to a heating rate of $\dot{n} = \Omega_g/100\pi$ versus $2\pi/\Omega_g t_G$ for the IDD-single, IDD-1, and IDD-2 gates. Similarly, in Fig. 4(b) we compare the same set of gates for a motional dephasing rate of $\Gamma_g = \Omega_g/100\pi$. Both calculations in Fig. 4 show that, while better than the IDD-single, the IDD-1 gate is not as robust as the IDD-2 gate; this can be understood because the IDD-1 trajectory is not centered on the origin of phase space. For $j > 2$, however, we find that there is not a significant improvement of $\mathcal{F}$ versus t_G relative to $j = 2$. This is because the phase-space trajectories of the IDD-j gates with $j > 1$ are all centered on the origin, thus saturating improvement to the time-averaged spin-motion entanglement.

VI. RESIDUAL MAGNETIC FIELD FROM THE GRADIENT

Generating a gradient that oscillates at ω_g typically leads to a residual magnetic field that also oscillates at ω_g. We represent the Hamiltonian of this residual magnetic field as

$$\hat{H}_z(t) = 2\hbar\Omega_z \cos(\omega_g t)\hat{S}_z, \tag{10}$$

which adds to the full Hamiltonian, given by Eq. (2). To analyze this field's effect on our gate, we make the transformation

given by Eq. (4). This gives

$$\hat{H}_{z,I}(t) = 2\hbar\Omega_z \cos(\omega_g t)$$

$$\times \left\{ \hat{S}_z\left[J_0\left(\frac{4\Omega_\mu}{\delta}\right) + 2\sum_{n=1}^{\infty} J_{2n}\left(\frac{4\Omega_\mu}{\delta}\right)\cos(2n\delta t) \right] \right.$$

$$\left. + 2\hat{S}_y \sum_{n=1}^{\infty} J_{2n-1}\left(\frac{4\Omega_\mu}{\delta}\right)\sin([2n-1]\delta t) \right\}. \tag{11}$$

Assuming $\Omega_z \ll \delta$, we can simplify this equation by dropping far-off-resonant terms. By solving Eq. (6), we find that

$$\delta = \frac{\omega_g}{2} - \frac{\Delta}{4}. \tag{12}$$

Keeping only the near-resonant terms gives

$$\hat{H}_{I,z}(t) \simeq 2\hbar\Omega_z J_2\left(\frac{4\Omega_\mu}{\delta}\right)\cos(\Delta t/2)\hat{S}_z. \tag{13}$$

Since the residual term is $\propto \hat{S}_z$, it commutes with the gate, and its effect at the end of a single-loop gate, $t_G = 2\pi/\Delta$, can be described by a unitary operator given by

$$\hat{U}_z(t) = \exp\left[-\frac{i}{\hbar} \int_0^{t_G} dt' H_{I,z}(t') \right]$$

$$= \exp\left[-\frac{4i\Omega_z}{\Delta} J_2\left(\frac{4\Omega_\mu}{\delta}\right)\sin(\pi)\hat{S}_z \right]$$

$$= \hat{I}. \tag{14}$$

Thus, a residual homogeneous magnetic field at ω_g (such that $\Omega_z \ll \delta$) does not impact the fidelity of the gate. For the gates described in this work, the J_4 and J_8 resonances were chosen specifically because the near-resonant ($\sim\omega_g$) contributions are $\propto \hat{S}_z$ [see Eq. (11)]. One could imagine a similar scheme using the $\omega_r \pm \omega_g$ sidebands and the J_2 and J_4 resonances. This, however, results in an on-resonant term $\propto \hat{S}_x$ in $H_{I,z}$, as opposed to the term $\propto \hat{S}_z$ in the J_4, J_8 gate. Since this term does not commute with the gate, it would have to be nulled in order to not affect the fidelity, which would make the scheme significantly more difficult to implement.

VII. POLYCHROMATIC GATES WITH MULTIPLE MICROWAVE PAIRS

The gate presented in this work shows resilience to motional decoherence similar to that of the laser-free polychromatic gate successfully demonstrated by Webb *et al.* [19], but it also has important advantages. In their experiment, Webb *et al.* implemented laser-free polychromatic gates by tuning two bichromatic microwave pairs close to the frequency of the sideband of a static gradient ($\omega_g = 0$). This scheme requires a total of 12 oscillating control fields plus a strong static magnetic field gradient [19], whereas the scheme presented here requires only two oscillating control fields, plus a strong, oscillating magnetic field gradient. Importantly, the scheme of Ref. [19] produces unavoidable errors outside the $\Omega_\mu/\omega_r \ll 1$ regime, which limits the achievable gate speed, while our gate scheme has no such limitation. We derive this result using our interaction picture formalism described in the Appendix C.
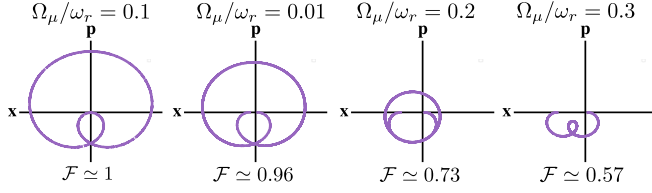
FIG. 5. Phase-space trajectories and fidelities $\mathcal{F}$, calculated using Eq. (2), for increasing values of Ω_μ/ω_r, where Ω_μ is the microwave strength and ω_r is the motional frequency. Even without imperfections, when $\Omega_\mu \sim \omega_r$, the phase-space trajectory distorts, and the value of $\mathcal{F}$ decreases.

Outside of this regime, terms that are higher order in Ω_μ/ω_r, as seen in Eq. (C4), contribute to the dynamics and distort the phase-space trajectory. In particular, the appearance of terms that oscillate at exactly ω_r prevents the motion from returning to its original state, leaving residual entanglement. This suggests that the implementation in Ref. [19] is limited to the weak microwave field regime. We illustrate this effect in Fig. 5, where we simulate the trajectory of Eq. (C4) for a static gradient with increasing values of Ω_μ, with no added noise. We can see that for the $\Omega_\mu/\omega_r \ll 1$ regime, the phase-space trajectory follows the two-tone trajectory described in Ref. [37] and $\mathcal{F} \to 1$. When $\Omega_\mu/\omega_r \sim 1$, however, the trajectory becomes distorted, and the gate fidelity decreases. Since the speed of the gate in the $\Omega_\mu \ll \delta$ regime is $\propto \Omega_\mu$, this indicates that for a limited value of Ω_g—typically the case in laser-free experiments—the maximum speed of a polychromatic gate performed via multiple pairs of microwave fields is slower than can be achieved with the oscillating gradient method presented here.

VIII. CONCLUSION

In this work, we described a laser-free trapped-ion entangling gate that can be tuned to be simultaneously robust to motional decoherence and qubit frequency shifts. The gate requires only two microwave magnetic fields and one near-motional-frequency magnetic field gradient. In addition to using analytic expressions, we numerically demonstrated this robustness. The design should enable higher gate fidelities for laser-free entangling gates without substantially increasing gate duration or the complexity of the required driving fields. We further demonstrated the advantages of our gate by showing that generating laser-free, polychromatic entangling gates using multiple pairs of microwave fields grows increasingly difficult when the microwave Rabi frequencies become comparable to the trap's secular frequency.

ACKNOWLEDGMENTS

APPENDIX A: LASER-FREE HAMILTONIAN

We consider a general Hamiltonian for laser-free gates between two trapped ions with identical qubit frequencies:

$$
\begin{aligned}
\hat{H}_{\text{lab}}(t) = &\frac{\hbar\omega_0}{2}\hat{S}_z + \hbar\omega_r\hat{a}^\dagger\hat{a} + 2\hbar\Omega_g f(t)\hat{S}_j\{\hat{a} + \hat{a}^\dagger\} \\
&+ 2\hbar\Omega_\mu\hat{S}_i \sum_n c_n\{\cos([\omega_0 + \delta_n]t) \\
&+ \cos([\omega_0 - \delta_n]t)\},
\end{aligned} \tag{A1}
$$

where $i \in \{x, y\}$ and $j \in \{x, y, z\}$. We define two-ion Pauli spin operators as $\hat{S}_\gamma \equiv \hat{\sigma}_{\gamma,1} + \hat{\sigma}_{\gamma,2}$. We have taken z to be the qubit quantization axis and ω_0 to be the qubit frequency. Here, we have assumed an ion crystal whose internal states are coupled via a motional mode with frequency ω_r and creation (annihilation) operators $\hat{a}^\dagger$ ($\hat{a}$). As they appear in this equation, Ω_μ and Ω_g are Rabi frequencies. Here, c_n is the amplitude (order unity) of the nth pair of equal amplitude fields, symmetrically detuned from the qubit frequency by $\pm\delta_n$. The Ω_g term describes the gradient-induced coupling of the internal states to the motion. The time-dependent function of the gradient $f(t)$ can be arbitrary; here, we take it to be constant or sinusoidally oscillating with a frequency of the same order of magnitude as ω_r.

We transform Eq. (A1) into the interaction picture with respect to the harmonic motion and qubit frequency terms, $\hat{H}_0 = \hbar\omega_0\hat{S}_z/2 + \hbar\omega_r\hat{a}^\dagger\hat{a}$. Furthermore, we make the rotating-wave approximation to eliminate terms oscillating with frequencies near $2\omega_0$. This gives the interaction Hamiltonian:

$$
\begin{aligned}
\hat{H}(t) = &2\hbar\Omega_\mu\hat{S}_i \sum_n c_n \cos(\delta_n t) \\
&+ 2\hbar\Omega_g f(t)\hat{S}_j\{\hat{a}e^{-i\omega_r t} + \hat{a}^\dagger e^{i\omega_r t}\}, \tag{A2}
\end{aligned}
$$

which is Eq. (2) from the main text when $i = x$ and $j = z$. Note that when $j \in \{x, y\}$, $f(t)$ changes from Eq. (A1) to Eq. (A2) when frequencies near $2\omega_0$ are dropped (see Ref. [27] for more details).

APPENDIX B: BICHROMATIC INTERACTION PICTURE

For completeness, we summarize an analysis of geometric phase gates for large microwave magnetic fields ($\Omega_\mu \sim \omega_r$) demonstrated originally in Ref. [27]. Assuming a Hamiltonian that takes the form of Eq. (2), representing a system with a bichromatic magnetic field pair and a (static or oscillatory) magnetic field gradient, we obtain

$$
\begin{aligned}
\hat{H}(t) = &\hat{H}_\mu(t) + \hat{H}_g(t) \\
= &2\hbar\Omega_\mu\hat{S}_i \cos(\delta t) + 2\hbar\Omega_g f(t)\hat{S}_j\{\hat{a}e^{-i\omega_r t} + \hat{a}^\dagger e^{i\omega_r t}\},
\end{aligned} \tag{B1}
$$

where we have dropped the subscript of δ since there is only one microwave pair. In order to exactly account for the dynamics caused by the larger of the two terms in this equation [$\hat{H}_\mu(t)$, the bichromatic field term], we note that the time propagator for this field alone is exactly solvable:

$$\hat{U}(t) = \exp\left[-2i\Omega_\mu \hat{S}_i \int_0^t dt' \cos(\delta t')\right]$$
$$= \exp\left[-\frac{2i\Omega_\mu}{\delta}\sin(\delta t)\hat{S}_i\right]. \quad (B2)$$

We can then transform into the interaction picture with respect to the bichromatic microwave term:

$$\hat{H}_I = \hat{U}^\dagger(t)\hat{H}_g(t)\hat{U}(t)$$
$$= 2\hbar\Omega_g f(t)\{\hat{a}e^{-i\omega_r t} + \hat{a}^\dagger e^{i\omega_r t}\}\hat{U}^\dagger(t)\hat{S}_j\hat{U}(t). \quad (B3)$$

Applying the Jacobi-Anger expansion (see Ref. [27]),

$$\hat{U}^\dagger(t)\hat{S}_j\hat{U}(t)$$
$$= \left\{\hat{S}_j\left[J_0\left(\frac{4\Omega_\mu}{\delta}\right) + 2\sum_{n=1}^\infty J_{2n}\left(\frac{4\Omega_\mu}{\delta}\right)\cos(2n\delta t)\right]\right.$$
$$\left. - 2\epsilon_{ijk}\hat{S}_k\sum_{n=1}^\infty J_{2n-1}\left(\frac{4\Omega_\mu}{\delta}\right)\sin([2n-1]\delta t)\right\}, \quad (B4)$$

giving

$$\hat{H}_I(t) = 2\hbar\Omega_g f(t)\{\hat{a}e^{-i\omega_r t} + \hat{a}^\dagger e^{i\omega_r t}\}$$
$$\times\left\{\hat{S}_j\left[J_0\left(\frac{4\Omega_\mu}{\delta}\right) + 2\sum_{n=1}^\infty J_{2n}\left(\frac{4\Omega_\mu}{\delta}\right)\cos(2n\delta t)\right]\right.$$
$$\left. - 2\epsilon_{ijk}\hat{S}_k\sum_{n=1}^\infty J_{2n-1}\left(\frac{4\Omega_\mu}{\delta}\right)\sin([2n-1]\delta t)\right\}. \quad (B5)$$

This shows a series of resonances corresponding to $\hat{\sigma}_z\hat{\sigma}_z$ and $\hat{\sigma}_\varphi\hat{\sigma}_\varphi$ (Mølmer-Sørensen) gates when the sideband frequency is an even or odd integer multiple of δ, respectively.

APPENDIX C: POLYCHROMATIC GATES WITH MULTIPLE PAIRS OF MICROWAVES

The Hamiltonian for the system containing multiple microwaves pairs used in [19] is given by

$$\hat{H}(t) = \hat{H}_{\mu,1}(t) + \hat{H}_{\mu,2} + \hat{H}_g(t)$$
$$= 2\hbar\Omega_\mu \hat{S}_x c_1\cos(\delta_1 t) + 2\hbar\Omega_\mu\hat{S}_x c_2\cos(\delta_2 t)$$
$$+ 2\hbar\Omega_g\hat{S}_z\{\hat{a}e^{-i\omega_r t} + \hat{a}^\dagger e^{i\omega_r t}\}. \quad (C1)$$

It is helpful to study the dynamics in the interaction picture with respect to both of the microwave field terms, which are exact. This gives

$$H_I(t) = \hat{U}_1^\dagger(t)\hat{U}_2^\dagger(t)\hat{H}_g(t)\hat{U}_2(t)\hat{U}_1(t), \quad (C2)$$

where

$$U_j(t) = \exp\left[-\frac{i}{\hbar}\int_0^t dt' H_{\mu,j}(t')\right]$$
$$= \exp\left[-\frac{2i\Omega_\mu c_j}{\delta_j}\sin(\delta_j t)\hat{S}_x\right]. \quad (C3)$$

Focusing on the Pauli operators and using Eq. (B4) twice, we obtain

$$\hat{U}_1^\dagger(t)\hat{U}_2^\dagger(t)\hat{S}_z\hat{U}_2(t)\hat{U}_1(t)$$
$$= \hat{S}_z\left\{\left[J_0\left(\frac{4\Omega_\mu c_1}{\delta_1}\right) + 2\sum_{n=1}^\infty J_{2n}\left(\frac{4\Omega_\mu c_1}{\delta_1}\right)\cos(2n\delta_1 t)\right]\right.$$
$$\times\left[J_0\left(\frac{4\Omega_\mu c_2}{\delta_2}\right) + 2\sum_{n=1}^\infty J_{2n}\left(\frac{4\Omega_\mu c_2}{\delta_2}\right)\cos(2n\delta_2 t)\right]$$
$$- 4\sum_{n,n'=1}^\infty J_{2n-1}\left(\frac{4\Omega_\mu c_1}{\delta_1}\right)J_{2n'-1}\left(\frac{4\Omega_\mu c_2}{\delta_2}\right)$$
$$\times\sin([2n-1]\delta_1 t)\sin([2n'-1]\delta_2 t)\Big\}$$
$$+ 2\hat{S}_y\left\{\left[\sum_{n=1}^\infty J_{2n-1}\left(\frac{4\Omega_\mu c_1}{\delta_1}\right)\sin([2n-1]\delta_1 t)\right]\right.$$
$$\times\left[J_0\left(\frac{4\Omega_\mu c_2}{\delta_2}\right) + 2\sum_{n=1}^\infty J_{2n}\left(\frac{4\Omega_\mu c_2}{\delta_2}\right)\cos(2n\delta_2 t)\right]$$
$$+ \left[\sum_{n=1}^\infty J_{2n-1}\left(\frac{4\Omega_\mu c_2}{\delta_2}\right)\sin([2n-1]\delta_2 t)\right]$$
$$\times\left[J_0\left(\frac{4\Omega_\mu c_1}{\delta_1}\right) + 2\sum_{n=1}^\infty J_{2n}\left(\frac{4\Omega_\mu c_1}{\delta_1}\right)\cos(2n\delta_1 t)\right]\Big\}. \quad (C4)$$

This equation can be simplified for the case considered by Webb *et al.* [19], where $\Omega_\mu \ll \omega_r$, $\delta_1 = \omega_r - \Delta$, $\delta_2 = \omega_r - 2\Delta$. Here, Δ is of the same order as Ω_g. Noting that $J_n(x) \to (\frac{x}{2})^n/n!$ as $x \to 0$ and keeping only the terms that are first order in Ω_μ/ω_r, we obtain

$$\hat{U}_1^\dagger(t)\hat{U}_2^\dagger(t)\hat{S}_z\hat{U}_2(t)\hat{U}_1(t) \simeq \hat{S}_z + \frac{4\Omega_\mu}{\omega_r}\hat{S}_y\{c_1\sin([\omega_r - \Delta]t)$$
$$+ c_2\sin([\omega_r - 2\Delta]t)\}, \quad (C5)$$

which, if we neglect the terms oscillating at frequencies on the order of ω_r, we get an interaction picture Hamiltonian:

$$\hat{H}_I(t) = \frac{4i\hbar\Omega_\mu\Omega_g}{\omega_r}\hat{S}_y\{\hat{a}^\dagger(c_1 e^{i\Delta t} + c_2 e^{2i\Delta t})$$
$$- \hat{a}(c_1 e^{-i\Delta t} + c_2 e^{-2i\Delta t})\}, \quad (C6)$$

giving the form of a polychromatic gate [37]. This means that in the $\Omega_\mu \ll \omega_r$ limit, as is the case in Ref. [19], this is a valid technique for performing laser-free polychromatic gates. If terms in Eq. (C4) that are higher order in Ω_μ/ω_r contribute,

terms that oscillate at exactly ω_r appear, such as

$$J_1\left(\frac{4\Omega_\mu c_2}{\omega_r}\right)J_2\left(\frac{4\Omega_\mu c_1}{\omega_r}\right)\sin([\omega_r - 2\Delta]t)\cos(2[\omega_r - \Delta]t)$$

$$= J_1\left(\frac{4\Omega_\mu c_2}{\omega_r}\right)J_2\left(\frac{4\Omega_\mu c_1}{\omega_r}\right)\{\sin([3\omega_r - 4\Delta]t) - \sin(\omega_r t)\}.$$

$$(C7)$$

These terms, as discussed in the text, prevent the trajectory from returning to the origin in phase space.

APPENDIX D: DECOHERENCE DUE TO BATH COUPLING

In this Appendix, we show that for the system described in the paper, we can calculate the infidelities due to Markovian heating and motional dephasing by numerically calculating the (significantly less computationally intensive) master equation for $\hat{H}_I$ (neglecting terms rotating near ω_r) rather than the full Hamiltonian given by Eq. (2). This is because the unitary transformation given by Eq. (4) commutes with the Lindblad operators that represent heating and motional dephasing. The full master equation for the time evolution of the full Hamiltonian, Eq. (2), including heating and motional dephasing, is

$$\dot{\hat{\rho}}(t) = -\frac{i}{\hbar}[\hat{H}(t), \hat{\rho}(t)] + \dot{\bar{n}}\left\{\hat{a}\hat{\rho}(t)\hat{a}^\dagger + \hat{a}^\dagger\hat{\rho}(t)\hat{a}\right.$$
$$\left. - \frac{1}{2}(\hat{a}^\dagger\hat{a} + \hat{a}\hat{a}^\dagger)\hat{\rho}(t) - \frac{1}{2}\hat{\rho}(t)(\hat{a}^\dagger\hat{a} + \hat{a}\hat{a}^\dagger)\right\}$$
$$+ \Gamma_d\left\{\hat{a}^\dagger\hat{a}\hat{\rho}(t)\hat{a}^\dagger\hat{a} - \frac{1}{2}(\hat{a}^\dagger\hat{a})^2\hat{\rho}(t) - \frac{1}{2}\hat{\rho}(t)(\hat{a}^\dagger\hat{a})^2\right\},$$

$$(D1)$$

where $\dot{\bar{n}}$ is the heating rate of the system and Γ_d is the motional dephasing rate. Making the unitary transformation defined by Eq. (4), we can solve for the density matrix in the interaction picture:

$$\hat{\rho}_I(t) = \hat{U}^\dagger(t)\hat{\rho}(t)\hat{U}(t). \qquad (D2)$$

Since the above transformation commutes with both the heating and motional dephasing operators, the interaction picture master equation is simply

$$\dot{\hat{\rho}}_I(t) = -\frac{i}{\hbar}[\hat{H}_I(t), \hat{\rho}_I(t)] + \dot{\bar{n}}\left\{\hat{a}\hat{\rho}_I(t)\hat{a}^\dagger + \hat{a}^\dagger\hat{\rho}_I(t)\hat{a}\right.$$
$$\left. - \frac{1}{2}(\hat{a}^\dagger\hat{a} + \hat{a}\hat{a}^\dagger)\hat{\rho}_I(t) - \frac{1}{2}\hat{\rho}_I(t)(\hat{a}^\dagger\hat{a} + \hat{a}\hat{a}^\dagger)\right\}$$
$$+ \Gamma_d\left\{\hat{a}^\dagger\hat{a}\hat{\rho}_I(t)\hat{a}^\dagger\hat{a} - \frac{1}{2}(\hat{a}^\dagger\hat{a})^2\hat{\rho}_I(t) - \frac{1}{2}\hat{\rho}_I(t)(\hat{a}^\dagger\hat{a})^2\right\}.$$

$$(D3)$$

The fast-rotating terms in H_I can be dropped with an effect scaling $\propto(\Omega_g/\omega_r)^2$. This is demonstrated by the calculations of the full numerical Hamiltonian shown for the pure state systems in this work. Numerically integrating Eq. (2) allows us to calculate $\hat{\rho}_I(t_G)$, where t_G is the gate duration, while accurately including the effects of Markovian heating and motional dephasing. As with the pure-state calculations, when $\hat{U}(t_G) \to \hat{I}$, $\hat{\rho}_I(t_G) \to \hat{\rho}(t_G)$, meaning that our reduced calculation gives the same answer as performing the full numerical integration of Eq. (D1) would, as long as the pure-state calculation is also valid.

[1] J. I. Cirac and P. Zoller, Quantum Computations with Cold Trapped Ions, Phys. Rev. Lett. **74**, 4091 (1995).

[2] C. Monroe, D. M. Meekhof, B. E. King, W. M. Itano, and D. J. Wineland, Demonstration of a Fundamental Quantum Logic Gate, Phys. Rev. Lett. **75**, 4714 (1995).

[3] M. A. Nielsen and I. L. Chuang, *Quantum Computation and Quantum Information* (Cambridge University Press, Cambridge, 2010).

[4] H. Häffner, C. F. Roos, and R. Blatt, Quantum computing with trapped ions, Phys. Rep. **469**, 155 (2008).

[5] R. Blatt and D. J. Wineland, Entangled states of trapped atomic ions, Nature (London) **453**, 1008 (2008).

[6] T. P. Harty, D. T. C. Allcock, C. J. Ballance, L. Guidoni, H. A. Janacek, N. M. Linke, D. N. Stacey, and D. M. Lucas, High-Fidelity Preparation, Gates, Memory, and Readout of a Trapped-Ion Quantum Bit, Phys. Rev. Lett. **113**, 220501 (2014).

[7] C. J. Ballance, T. P. Harty, N. M. Linke, M. A. Sepiol, and D. M. Lucas, High-Fidelity Quantum Logic Gates Using Trapped-Ion Hyperfine Qubits, Phys. Rev. Lett. **117**, 060504 (2016).

[8] J. P. Gaebler, T. R. Tan, Y. Lin, Y. Wan, R. Bowler, A. C. Keith, S. Glancy, K. Coakley, E. Knill, D. Leibfried, and D. J. Wineland, High-Fidelity Universal Gate Set for ^{9}Be$^+$ Ion Qubits, Phys. Rev. Lett. **117**, 060505 (2016).

[9] D. J. Wineland, C. Monroe, W. M. Itano, D. Leibfried, B. E. King, and D. M. Meekhof, Experimental issues in coherent quantum-state manipulation of trapped atomic ions, J. Res. Natl. Inst. Stand. Technol. **103**, 259 (1998).

[10] K. Mølmer and A. Sørensen, Multiparticle Entanglement of Hot Trapped Ions, Phys. Rev. Lett. **82**, 1835 (1999).

[11] A. Sørensen and K. Mølmer, Entanglement and quantum computation with ions in thermal motion, Phys. Rev. A **62**, 022311 (2000).

[12] D. Leibfried, B. DeMarco, V. Meyer, D. M. Lucas, M. Barrett, J. Britton, W. M. Itano, B. Jelenković, C. Langer, T. Rosenband, and D. J. Wineland, Experimental demonstration of a robust, high-fidelity geometric two ion-qubit phase gate, Nature (London) **422**, 412 (2003).

[13] R. Ozeri, W. M. Itano, R. B. Blakestad, J. Britton, J. Chiaverini, J. D. Jost, C. Langer, D. Leibfried, R. Reichle, S. Seidelin, J. H. Wesenberg, and D. J. Wineland, Errors in trapped-ion quantum gates due to spontaneous photon scattering, Phys. Rev. A **75**, 042329 (2007).

[14] F. Mintert and C. Wunderlich, Ion-Trap Quantum Logic Using Long-Wavelength Radiation, Phys. Rev. Lett. **87**, 257904 (2001).

[15] A. Khromova, Ch. Piltz, B. Scharfenberger, T. F. Gloger, M. Johanning, A. F. Varón, and C. Wunderlich, Designer Spin Pseudomolecule Implemented with Trapped Ions in a Magnetic Gradient, Phys. Rev. Lett. **108**, 220502 (2012).

[16] K. Lake, S. Weidt, J. Randall, E. D. Standing, S. C. Webster, and W. K. Hensinger, Generation of spin-motion entanglement in a trapped ion using long-wavelength radiation, Phys. Rev. A **91**, 012319 (2015).

[17] J. Randall, S. Weidt, E. D. Standing, K. Lake, S. C. Webster, D. F. Murgia, T. Navickas, K. Roth, and W. K. Hensinger, Efficient preparation and detection of microwave dressed-state qubits and qutrits with trapped ions, Phys. Rev. A **91**, 012322 (2015).

[18] S. Weidt, J. Randall, S. C. Webster, K. Lake, A. E. Webb, I. Cohen, T. Navickas, B. Lekitsch, A. Retzker, and W. K. Hensinger, Trapped-Ion Quantum Logic with Global Radiation Fields, Phys. Rev. Lett. **117**, 220501 (2016).

[19] A. E. Webb, S. C. Webster, S. Collingbourne, D. Bretaud, A. M. Lawrence, S. Weidt, F. Mintert, and W. K. Hensinger, Resilient Entangling Gates for Trapped Ions, Phys. Rev. Lett. **121**, 180501 (2018).

[20] C. Ospelkaus, C. E. Langer, J. M. Amini, K. R. Brown, D. Leibfried, and D. J. Wineland, Trapped-Ion Quantum Logic Gates Based on Oscillating Magnetic Fields, Phys. Rev. Lett. **101**, 090502 (2008).

[21] C. Ospelkaus, U. Warring, Y. Colombe, K. R. Brown, J. M. Amini, D. Leibfried, and D. J. Wineland, Microwave quantum logic gates for trapped ions, Nature (London) **476**, 181 (2011).

[22] T. P. Harty, M. A. Sepiol, D. T. C. Allcock, C. J. Ballance, J. E. Tarlton, and D. M. Lucas, High-Fidelity Trapped-Ion Quantum Logic Using Near-Field Microwaves, Phys. Rev. Lett. **117**, 140501 (2016).

[23] S. Wölk and C. Wunderlich, Quantum dynamics of trapped ions in a. dynamic field gradient using dressed states, New J. Phys. **19**, 083021 (2017).

[24] H. Hahn, G. Zarantonello, M. Schulte, A. Bautista-Salvador, K. Hammerer, and C. Ospelkaus, Integrated $^9Be^+$ multi-qubit gate device for the ion-trap quantum computer, New J. Phys. Quantum Inf. **5**, 70 (2019).

[25] G. Zarantonello, H. Hahn, J. Morgner, M. Schulte, A. Bautista-Salvador, R. F. Werner, K. Hammerer, and C. Ospelkaus, Robust and Resource-Efficient Microwave Near-Field Entangling $^9Be^+$ Gate, Phys. Rev. Lett. **123**, 260503 (2019).

[26] J. Chiaverini and W. E. Lybarger, Laserless trapped-ion quantum simulations without spontaneous scattering using microtrap arrays, Phys. Rev. A **77**, 022324 (2008).

[27] R. T. Sutherland, R. Srinivas, S. C. Burd, D. Leibfried, A. C. Wilson, D. J. Wineland, D. T. C. Allcock, D. H. Slichter, and S. B. Libby, Versatile laser-free trapped-ion entangling gates, New J. Phys. **21**, 033033 (2019).

[28] R. Srinivas, S. C. Burd, R. T. Sutherland, A. C. Wilson, D. J. Wineland, D. Leibfried, D. T. C. Allcock, and D. H. Slichter, Trapped-Ion Spin-Motion Coupling with Microwaves and a Near-Motional Oscillating Magnetic Field Gradient, Phys. Rev. Lett. **122**, 163201 (2019).

[29] L. Viola and S. Lloyd, Dynamical suppression of decoherence in two-state quantum systems, Phys. Rev. A **58**, 2733 (1998).

[30] L. Viola, E. Knill, and S. Lloyd, Dynamical Decoupling of Open Quantum Systems, Phys. Rev. Lett. **82**, 2417 (1999).

[31] N. Timoney, I. Baumgart, M. Johanning, A. F. Varón, M. B. Plenio, A. Retzker, and C. Wunderlich, Quantum gates and memory using microwave-dressed states, Nature (London) **476**, 185 (2011).

[32] A. Bermudez, P. O. Schmidt, M. B. Plenio, and A. Retzker, Robust trapped-ion quantum logic gates by continuous dynamical decoupling, Phys. Rev. A **85**, 040302(R) (2012).

[33] M. Johanning, A. Braun, N. Timoney, V. Elman, W. Neuhauser, and C. Wunderlich, Individual Addressing of Trapped Ions and Coupling of Motional and Spin States Using rf Radiation, Phys. Rev. Lett. **102**, 073004 (2009).

[34] D. Hayes, S. M. Clark, S. Debnath, D. Hucul, I. V. Inlek, K. W. Lee, Q. Quraishi, and C. Monroe, Coherent Error Suppression in Multiqubit Entangling Gates, Phys. Rev. Lett. **109**, 020503 (2012).

[35] T. J. Green and M. J. Biercuk, Phase-Modulated Decoupling and Error Suppression in Qubit-Oscillator Systems, Phys. Rev. Lett. **114**, 120502 (2015).

[36] P. H. Leung, K. A. Landsman, C. Figgatt, N. M. Linke, C. Monroe, and K. R. Brown, Robust 2-Qubit Gates in a Linear Ion Crystal Using a Frequency-Modulated Driving Force, Phys. Rev. Lett. **120**, 020501 (2018).

[37] F. Haddadfarshi and F. Mintert, High fidelity quantum gates of trapped ions in the presence of motional heating, New J. Phys. **18**, 123007 (2016).

[38] Y. Shapira, R. Shaniv, T. Manovitz, N. Akerman, and R. Ozeri, Robust Entanglement Gates for Trapped-Ion Qubits, Phys. Rev. Lett. **121**, 180502 (2018).

[39] D. Jonathan, M. B. Plenio, and P. L. Knight, Fast quantum gates for cold trapped ions, Phys. Rev. A **62**, 042307 (2000).

[40] C. F. Roos, Ion trap quantum gates with amplitude-modulated laser beams, New J. Phys. **10**, 013002 (2008).

[41] R. B. Blackman and J. W. Tukey, The measurement of power spectra from the point of view of communications engineering—Part I, Bell Syst. Tech. J **37**, 185 (1958).

[42] H. Breuer and F. Petruccione, *The Theory of Open Quantum Systems* (Oxford University Press, Oxford, 2002).